NANO LETTERS

pubs.acs.org/NanoLett

Letter

Stable and Size Tunable $CsPbBr_3$ Nanocrystals Synthesized with Oleylphosphonic Acid

Baowei Zhang, Luca Goldoni, Chiara Lambruschini, Lisa Moni, Muhammad Imran, Andrea Pianetti, Valerio Pinchetti, Sergio Brovelli,* Luca De Trizio,* and Liberato Manna*

Cite This: *Nano Lett.* 2020, 20, 8847−8853

Read Online

ACCESS | Metrics & More | Article Recommendations | Supporting Information

ABSTRACT: We employed oleylphosphonic acid (OLPA) for the synthesis of $CsPbBr_3$ nanocrystals (NCs). Compared to phosphonic acids with linear alkyl chains, OLPA features a higher solubility in apolar solvents, allowing us to work at lower synthesis temperatures (100 °C), which in turn offer a good control over the NCs size. This can be reduced down to 5.0 nm, giving access to the strong quantum confinement regime. OLPA-based NCs form stable colloidal solutions at very low concentrations (∼1 nM), even when exposed to air. Such stability stems from the high solubility of OLPA in apolar solvents, which enables these molecules to reversibly bind/unbind to/from the NCs, preventing the NCs aggregation/precipitation. Small NCs feature efficient, blue-shifted emission and an ultraslow emission kinetics at cryogenic temperature, in striking difference to the fast decay of larger particles, suggesting that size-related exciton structure and/or trapping-detrapping dynamics determine the thermal equilibrium between coexisting radiative processes.

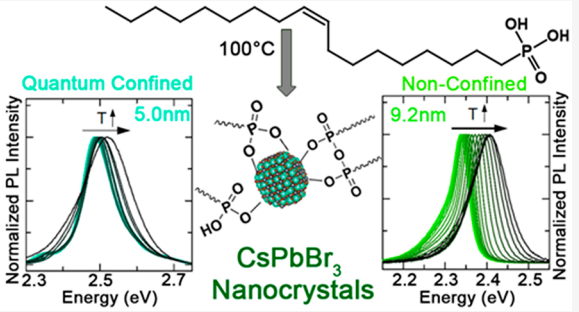

KEYWORDS: *oleylphosphonic acid, perovskite nanocrystals, NMR*

Lead halide perovskites (LHPs) nanocrystals (NCs) have drawn attention in the last five years due to their ideal optical properties which make them potential candidates in several applications including liquid crystal displays, light emitting diodes, solar concentrators and radiation detectors.[1−8] The efficient photoluminescence (PL) emission of LHP NCs stems from their intrinsic defect tolerant nature.[3,9,10] In these systems, various works have shown that their surface passivation, via a proper choice of surfactants, plays a fundamental role in achieving both colloidally stable and strongly emissive LHP NCs.[9,11] Aliphatic amines and carboxylic acids (most often oleylamine and oleic acid) are the standard ligands employed in the synthesis of these NCs, eventually passivating their surface as charged species (as ammonium and carboxylate ions, respectively). Various studies have demonstrated that a simple variation of the local pH, which can cause protonation/deprotonation of carboxylate/oleylammonium ions, or even a dilution of the NC suspension, which decreases the chemical potential of the free ligands with respect to that of bound ones, can lead to ligands detachment, which is deleterious for both colloidal stability and PL.[9,12] Consequently, these types of ligands are weakly bound to the NCs surface, and a highly dynamic equilibrium exists between free and bound ligands.[9,13−15] In order to optimize the surface passivation of LHP NCs, various alternative surfactants have been investigated, with zwitterionic molecules, quaternary alkyl ammonium ions, and sulfonic and alkyl phosphonic acids being the most promising ones.[3,9,12,16,17] The improved stability in these cases arises from the fact that either they cannot be deprotonated (zwitterionic molecules, quaternary alkylammonium ions), or they have a strong affinity toward surface Pb^{2+} ions (sulfonic and phosphonic acids). As a result, all these ligands yield LHP NCs with higher stability and near-unity PL quantum yield (QY).

In a recent work from our group, we demonstrated that $CsPbBr_3$ NCs, synthesized in the presence of alkyl phosphonic acids as the only ligands in the reaction environment, are very stable against dilution, maintaining ∼100% PLQY even at concentrations as low as ∼1 nM. These NCs were found to be coated by hydrogen phosphonate and phosphonic acid anhydride molecules, the latter formed *in situ*, during the NCs' synthesis. In these NCs, we could observe ligand desorption under an inert atmosphere, in the form of Pb-phosphonates, only when heating the NCs dispersions at temperatures of 50 °C or above.[12] Such stability stems from the strong binding affinity of the alkyl phosphonate species to Pb^{2+} cations at ambient temperature. On the other hand, that

Received: September 22, 2020
Revised: November 11, 2020
Published: November 17, 2020

https://dx.doi.org/10.1021/acs.nanolett.0c03833
Nano Lett. 2020, 20, 8847−8853

synthesis approach had two major limitations: (i) the NC dispersions turned out to be unstable in air; (ii) the phosphonic acids employed (namely tetradecyl- and octadecylphosphonic acids) require high temperatures (at least 220 °C or above) to solubilize the metal cation precursors and this prevented the synthesis of small NCs.[12] As a matter of fact, with that method we could not grow NCs with sizes smaller than ∼7 nm.

To overcome these issues, in this work we have developed a synthesis of $CsPbBr_3$ NCs that employs oleylphosphonic acid (OLPA) as the sole surfactant present in the reaction environment. The good solubility of OLPA in common apolar solvents allows for the solubilization of metal cation precursors at low temperatures (as low as 80 °C) which, in turn, enable the synthesis of $CsPbBr_3$ NCs with a good control over their mean size down to 5.0 nm (Scheme 1), thus accessing the

Scheme 1. Colloidal Synthesis of $CsPbBr_3$ NCs Employing Oleylphosphonic Acid

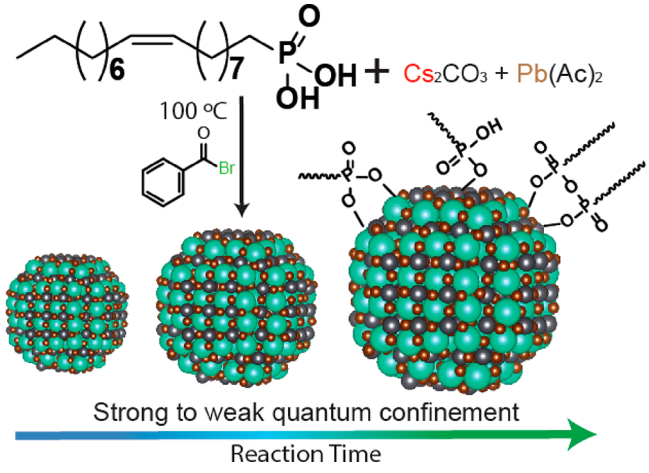

strong quantum confinement regime (the exciton Bohr diameter of $CsPbBr_3$ is 7 nm).[18,19] OLPA-based $CsPbBr_3$ NCs, which are passivated by hydrogen phosphonates, phosphonic acid anhydrides, and phosphonate species (Scheme 1), exhibit excellent colloidal stability even when exposed to air and at extremely low concentration (∼1 nM), with no need to avoid cleaning procedures or to perform postsynthesis ligand exchange treatments aimed at preventing size evolution, as done in previous works in which small $CsPbBr_3$ NCs were prepared and studied optically.[19,20]

Our PL measurements evidenced that quantum confined NCs feature highly efficient, blue-shifted emission with respect to bulk $CsPbBr_3$, and their kinetics slows down dramatically at cryogenic temperature, with no concomitant change of the PLQY. This radiative effect is markedly different from the accelerated decay with decreasing temperature commonly observed for larger NCs, which is ascribed to the presence of a bright triplet lowest excitonic state[21] and suggests an exciton fine structure featuring a low energy dark state in thermal equilibrium with a higher-lying bright state, in agreement with recent works.[20]

The $CsPbBr_3$ NCs of this work were prepared by modifying the colloidal approach that we recently reported.[12] In the present case, we synthesized OLPA (with the ratio of cis/trans isomers calculated to be roughly 72/28; see Figure S5 and the Supporting Information for details) and used it as the only surfactant to drastically reduce the temperature at which the metal cation precursors (Cs_2CO_3 and $Pb(ac)_2$) could be dissolved in octadecene (ODE). As a comparison, a complete dissolution (i.e., the formation of a transparent reactant solution) of metal precursors was observed only at 220 °C when working with either tetradecyl- or octadecylphosphonic acids, while in the case of OLPA this was achieved at 120 °C. Moreover, when using OLPA, the complexes that form during this step were soluble in ODE at temperatures as low as 80 °C, while those formed when employing tetradecyl- or octadecylphosphonic acids required at least 160 °C to completely dissolve.[12] This is due, most likely, to the fact that OLPA molecules are characterized by the presence of a double bond, so that intermolecular London forces are weaker and their melting points are lower than in the case of phosphonic acids with linear and saturated alkyl chains.[22,23] Three NC samples were prepared by performing the synthesis at 100 °C and varying the reaction time from 45 to 600 s (see the experimental section for details). The XRD analysis confirmed that all the NC products have the expected orthorhombic $CsPbBr_3$ perovskite structure (ICSD number 98751) with no presence of impurities (Figure 1d).

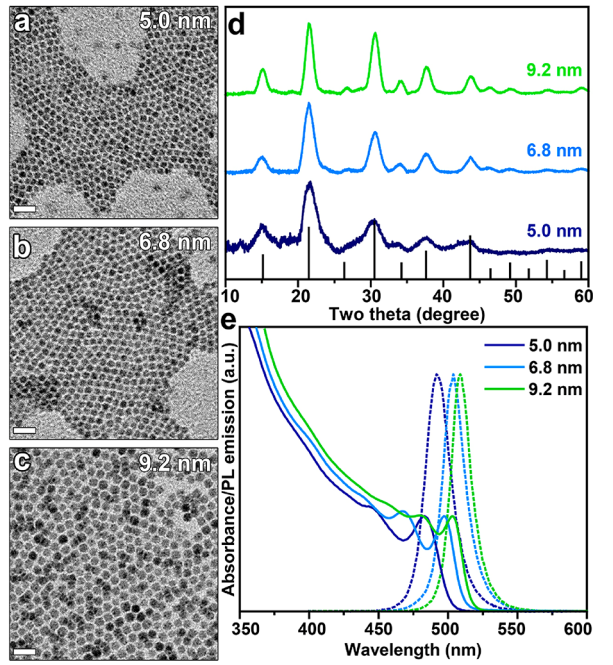

Figure 1. TEM images of (a) 5.0 nm, (b) 6.8 nm, and (c) 9.2 nm (green) OLPA-based $CsPbBr_3$ NCs. The scale bars are 50 nm. (d) XRD patterns of OLPA-based NC samples together with the bulk reflections of the orthorhombic $CsPbBr_3$ perovskite structure (ICSD number 98751). (e) Corresponding absorption and PL emission spectra of suspensions of the same three NC samples.

The TEM images indicated that the increase in reaction time from 45 to 600 s at 100 °C enables tuning the $CsPbBr_3$ NCs size from ∼5.0 to ∼9.2 nm (Figure 1a–c) with all the samples exhibiting a narrow size distribution (Figure S7). These OLPA-based NCs have a truncated octahedron shape, similarly to what we previously observed when using tetradecyl- or octadecyl- phosphonic acids in the synthesis.[12] This shape originates from the preferential binding affinity of alkylphosphonates to both (001) and (110) Pb-terminated facets.[12] As a further support to this, the XPS analysis indicated a Cs/Pb/Br/

https://dx.doi.org/10.1021/acs.nanolett.0c03833
Nano Lett. 2020, 20, 8847−8853

P ratio of 1/1.2/2.5/0.75, close to that measured in our previous work, which is consistent with $CsPbBr_3$ NCs having a Pb-rich surface termination, with part of Br ions being replaced by alkyl phosphonates, hydrogen phosphonates and phosphonic acid anyhdrides (ensuring charge balance).[12]

As a consequence of a broader range of accessible sizes with this method, the absorption and photoluminescence spectra of these samples can be tuned from 503 nm (PL maximum at 509 nm) in the case of 9.2 nm NCs to 482 nm (PL maximum at 491 nm) for 5.0 nm NCs (Figure 1e). The PLQYs of 5.0, 6.8, and 9.2 nm NCs are 91%, 84%, and 81%, respectively, indicating an efficient passivation of surface trap states. Moreover, according to our stability tests, such high PL emission was retained even when diluting the NCs dispersions down to 1−10 nM, also in the case of strongly quantum confined NCs (Figure S8). Such experiments highlight that OLPA-based NCs exhibit a high colloidal stability with ligands being strongly bound to the surface.[9,24,25] Another important feature of OLPA-based samples is that the colloidal dispersions of NCs are stable in air up to 2 weeks (Figure S9). This is a relevant improvement, considering that colloidal suspensions of NCs prepared with tetradecyl- or octadecylphosphonic acids are poorly stable in air: upon air exposure, the precipitation of NCs was observed together with the formation of an insoluble foam-like product (Figure S9). These results point to an improved stability of OLPA-based NCs, which is remarkable in the case of quantum confined ones (i.e., 5.0 nm).

With the aim of explaining the improved stability of OLPA-based NCs, and, in particular, that of quantum confined NCs, and to unveil the composition of their ligand shell, we thoroughly characterized them via NMR analysis. Both ^{1}H and ^{31}P NMR spectra of quantum confined LHP NCs evidenced the presence of P-based molecules bound to the surface of the NCs: both alkenyl protons (9,10) at 5.3 ppm (Figure 2a) and phosphorus signals peaks in the range 10−40 ppm (Figure 2b) were broadened with respect to those of free OLPA ligands (Figure S3 and S10), an indication that these P-based molecules have a longer correlation time (τ_c) as a consequence of their binding to NCs' surface.[23] Also, the presence of multiple ^{31}P signals was a mark of a complex ligand−surface interaction, with surface molecules adopting different binding motifs with Pb^{2+} cations.

To reveal how OLPA molecules were anchored to the surface of perovskite NCs, we treated our NCs with trimethylchlorosilane (TMS-Cl) and we analyzed the corresponding products via ^{31}P NMR. TMS-Cl and, in general, halides and chalcogenides (i.e., TMS-I, -Br, -Se, or -S) are known to react with phosphonate species bound to the surface of colloidal NCs delivering the corresponding TMS-substituted compounds (and leading to the precipitation of the NCs).[12,25−27] Upon reaction of OLPA-based NCs with TMS-Cl we observed the formation of free species being characterized by four individual ^{31}P NMR peaks (Figure 2c): one pair of sharp peaks at 14.92 and 15.52 ppm with similar intensities were assigned to *O,O′*-bis(trimethylsilyl)-oleylphosphonic acid anhydride diastereoisomers; the peaks at 33.95 and 16.65 ppm could be ascribed to mono- and di-TMS substituted OLPA species (namely, TMS hydrogen oleylphosphonic acid and *O,O′*-bis(TMS)oleylphosphonic acid), respectively (see also Figure S10).[12,26] Furthermore, the analysis of the ^{1}H NMR peaks ascribable to alkenyl protons of such species indicated a cis/trans isomer ratio of 65/35 (i.e., the portion of trans isomers slightly increased upon the synthesis; see Figure S6). These results indicate that the surface of the NCs was passivated by different species including phosphonates (PA^{2-}), hydrogen phosphonates (PA^-), and phosphonic acid anhydrides [PA(anhy)] (see the sketch in Figure 2b). The calculated PA^-/PA^{2-}/PA(anhy) ratios are 1/2.15/3.2 (that corresponds to a 1/1.02 ratio between phosphonate and anhydride species). Interestingly, PA^{2-} species were not observed in our previous work in which tetradecylphosphonic acid molecules were employed for the synthesis of LHP NCs at higher temperatures (180 °C) and where a PA^-/PA(anhy) ratio of 1/2.21 was detected (Figure S11).[12] Overall, our NMR studies suggest that low synthesis temperatures (i.e., 100 °C) promote the formation of deprotonated PA^- and especially PA^{2-} moieties rather than PA(anhy) ones (Figure S12). This was further supported by a control experiment in which we synthesized LHP NCs with OLPA at 160 °C: the ^{31}P NMR characterization in this case revealed the absence of PA^{2-} species, but only PA^- and PA(anhy) (Figures S13−15).

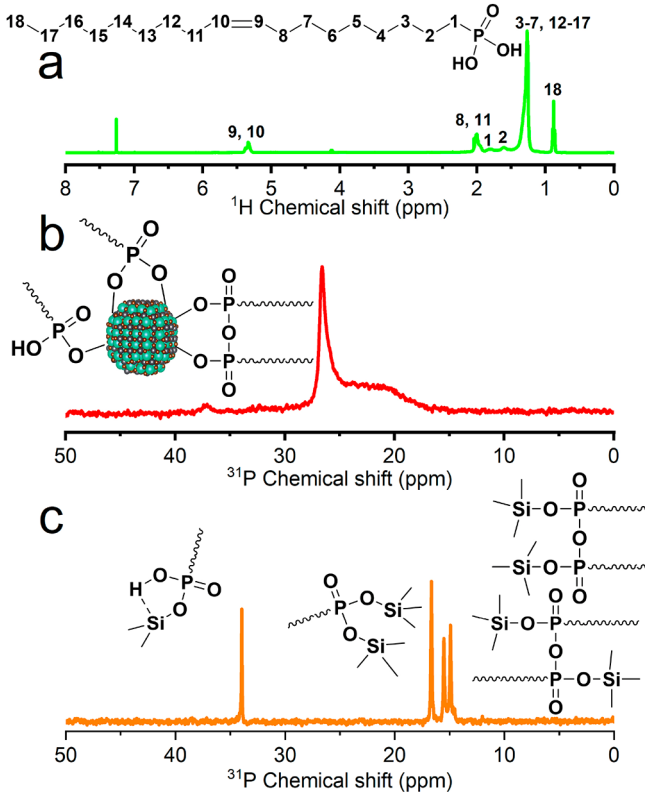

Figure 2. (a) ^{1}H NMR and (b) ^{31}P NMR spectra of quantum confined (5.0 nm) $CsPbBr_3$NCs dispersed in $CDCl_3$. (c) ^{31}P NMR spectrum in $CDCl_3$ of the products of the reaction between OLPA-based NCs and TMS-Cl.

Our results highlight that the reaction temperature plays a major role in dictating the binding motif of phosphonic acids on the surface of LHP and, presumably, metal halide NCs in general. On the other hand, the presence of PA^{2-} species on the surface of OLPA-based NCs is not sufficient to explain their improved stability under air. Indeed, as we previously calculated, the binding energies of PA^{2-} and PA^- species with surface Pb^{2+} cations are similar (47.9 and 52.2 kcal/mol, respectively).[12] One possible explanation for the stability of OLPA-based NCs in air can be attributed to the high solubility of OLPA molecules (and anhydrides) in apolar solvents. After

https://dx.doi.org/10.1021/acs.nanolett.0c03833
Nano Lett. 2020, 20, 8847−8853

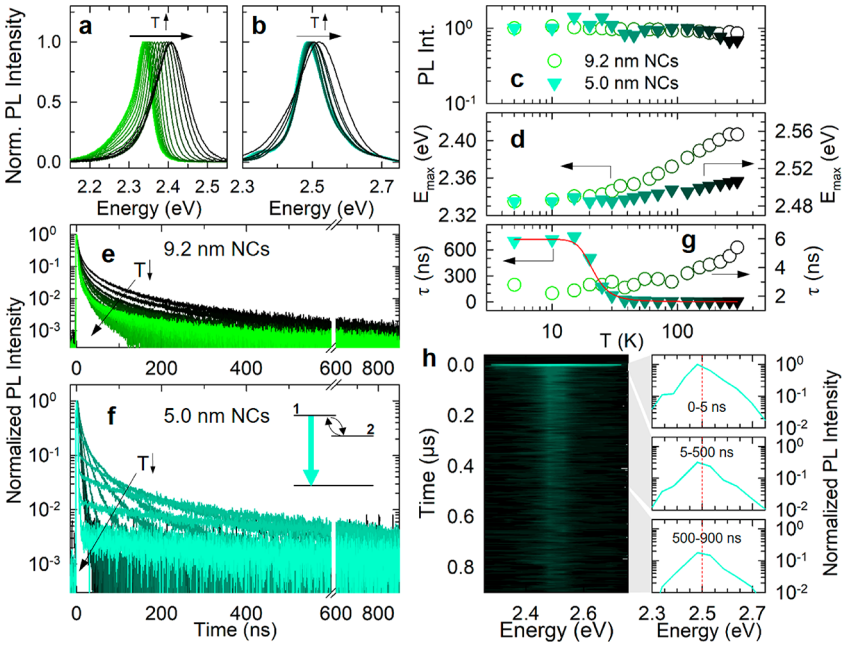

Figure 3. Normalized PL spectra of (a) 9.2 nm and (b) 5.0 nm OLPA-based $CsPbBr_3$ NCs as a function of temperature from T = 5 K (light green) to T = 300 K (dark green). Temperature dependence of (c) the PL intensity (normalized to the value at T = 5K) and (d) the PL energy position of the 9.2 and 5.0 nm NCs (circles and triangles, respectively). Normalized PL decay traces as a function of temperature of (e) 9.2 nm and (f) 5.0 nm NCs acquired at the PL peak. Inset: Sketch of the thermal equilibrium between a high-energy emissive state (1) and a lower-energy, nonemissive state (2). (g) Temperature dependences of the PL lifetimes. The red line is the result of the fitting procedure with eq 1 for the 5.0 nm NCs. (h) Contour plot of the PL emission of 5.0 nm NCs acquired at T = 5 K together with the respective PL spectra as extracted by integrating in the 0−5 ns (top panel), 5−500 ns (middle panel), and 500−900 ns (bottom panel) ranges. The same color scheme applies to all panels.

the exposure to air, oleyl phosphonates (and anhydrides) can be protonated by water molecules and, thus, partially released from the NC surface and solubilized by the solvent. Being still in solution they can rebind to the surface of the NCs in a dynamic fashion. Such hypothesis was supported by a control experiment in which we dispersed OLPA-based NCs into non-anhydrous $CDCl_3$, added a stoichiometric amount of OLPA molecules (9 mmol of OLPA per mmol of NCs), and analyzed the corresponding dispersions via NMR (see the Supporting Information for details). The analyses indicate that neutral OLPA molecules are capable of dynamically binding the surface of the NCs. Conversely, phosphonic acids with linear alkyl chains (such as tetradecyl- or octadecylphosphonic acids), once protonated (again, upon exposure of the NC dispersion to air), are not soluble in apolar solvent, forming an insoluble gel (Figure S9); hence they cannot participate to the surface passivation of the NCs anymore. In this case, the NCs become progressively deprived of surface ligands and start aggregating.

The stability that characterizes even the small, strongly quantum confined $CsPbBr_3$ NCs that are accessible through this synthesis, with no need of postsynthesis ligand treatment,[19,20] presents us with a unique opportunity to study the optical properties of these materials in the strong confinement regime. We therefore proceeded to investigate the optical properties of both non- (9.2 nm) and quantum- (5.0 nm) confined OLPA-based NCs via side-by-side PL measurements as a function of temperature. Upon lowering the temperature, the PL spectra of both samples progressively red-shifted (Figure 3a,b), as expected due to bandgap renormalization,[28−33] and their PL intensity remained essentially constant (Figure 3c), in agreement with the near-unity PLQY measured at RT and confirming excellent passivation of surface traps.

Consistent with the smaller number of atoms involved in the thermal expansion of the perovskite crystal lattice upon lowering the temperature, the red shift of the PL maximum was less pronounced for the 5.0 nm NCs than for the 9.2 nm ones (∼30 meV vs ∼80 meV, respectively, Figure 3a,b,d).

The most striking difference between the optical properties of small vs weakly confined NCs was found by comparing the temperature evolution of the respective PL kinetics reported in Figure 3e,f. At room temperature, both systems showed a nearly single-exponential dynamics with lifetime (τ) of ∼5 ns. Upon lowering the temperature, the PL dynamics of the 9.2 NCs progressively accelerated, reaching τ ∼2.5 ns at T = 5 K (Figure 3e,g). This effect is typical of LHP NCs with a lateral size of 8−15 nm and has been ascribed to the radiative decay of bright triplet excitons becoming dominant at cryogenic temperatures.[21,33,34] On the other hand, the evolution of the PL kinetics of the 5.0 nm NCs was substantially different: for 300 K < T < 50 K, the PL lifetime gradually lengthened, reaching τ ∼13 ns at 50 K; at lower temperatures (i.e., < 50 K), the PL decay was characterized by a marked double exponential kinetics, with a fast resolution-limited component followed by a slow PL with τ ∼700 ns (at 5 K), over 2 orders of magnitude longer than that at room temperature (Figure 3f). Importantly, no concomitant change of the PL intensity was observed (Figure 3c), indicating that such a double exponential decay kinetics originates from purely radiative effects. As sketched in the inset of Figure 3f, this behavior can be described by the thermal equilibrium between two states: a higher energy excitonic state (labeled as **1**) with a large oscillator strength responsible for the fast decay at room temperature and a lower lying state (labeled as **2**), weakly optically coupled to the ground state, that determines the slow PL kinetics below 20 K. At high temperatures, state **1** is

https://dx.doi.org/10.1021/acs.nanolett.0c03833
Nano Lett. 2020, 20, 8847−8853

thermally populated, and the respective fast PL, thus, dominates the emission. Upon lowering the temperature, excitons thermalized into state **2** could no longer be promoted to state **1**, resulting in the very slow PL tail. Consistent with this picture, we adequately fitted the trend of τ as a function of temperature with the equation

$$\tau(T) = (1 + \exp(-\Delta_{1,2}/k_B T)) / (\tau_1^{-1} + \tau_2^{-1} \exp(-\Delta_{1,2}/k_B T)) \quad (1)$$

where k_B is the Boltzmann constant, τ_1 and τ_2 are the PL lifetimes of state **1** and **2**, respectively, and $\Delta_{1,2}$ is the energy separation between these two states (Figure 3g). From the fitting procedure, we obtained $\Delta_{1,2}$ ~12 meV, which is significantly smaller than the PL line width of the NC ensemble. Consistently, the contour plot of the time-resolved PL of the 5.0 nm OLPA-based NCs showed no spectral modification over time. This effect can be better appreciated by looking at the PL spectra obtained by integrating the contour plot in the 0−5 ns (which is dominated by the resolution-limited component), 5−500 ns, and 500−900 ns time ranges, all featuring the same PL profile (Figure 3h).

All such observations, including comparable value for $\Delta_{1,2}$, agree with recent results on small $CsPbBr_3$ NCs, ascribing the long-lived PL tail at cryogenic temperatures to the radiative decay of a nonemissive or "dark" exciton state.[20] To date, such an interpretation is mostly based on the phenomenological similarity to the exciton fine structure effects commonly observed for strongly confined CdSe NCs, yet a detailed theoretical description of the exciton fine structure of quantum confined LHP NCs is still lacking. Therefore, our results could be of interest to extend the theoretical framework currently available for larger NCs (lateral size of 8−15 nm) through the above-mentioned bright-triplet model,[21] to more strongly confined NCs where the exciton fine structure could be substantially different. For completeness, we do not exclude that the observed phenomenology could also arise from the involvement of very shallow trap states that store the excitation at low temperature (via single carrier or exciton trapping) and slowly repopulate the band edge, leading to the long-lived PL tail. In this case, however, constant PLQY with decreasing temperature would require suppression, at identical temperatures, of nonradiative decay channels for long-lived trapped carriers and band edge excitons, which is unlikely to occur. The in-depth investigation of such a photophysical response and the nature of the involved electronic states is beyond the scope of this work and will be addressed in a dedicated study.

In summary, we synthesized $CsPbBr_3$ NCs using oleylphosphonic acid (OLPA), which allows us to lower the reaction temperature (100 °C) and make it possible to finely control the size, down to 5.0 nm, thus giving us access to NCs in the quantum confinement regime that are colloidally stable. OLPA-based NCs are passivated by different species, including phosphonates, hydrogen phosphonates, and phosphonic acid anhydrides, and form very stable colloidal solutions even at very low concentrations (1−10 nM) and when exposed to air. Side-by-side PL measurements at cryogenic temperatures evidenced striking differences in the low-temperature emission kinetics between quantum-confined OLPA-based NCs and larger NCs. Such differences are in agreement with recently invoked size-dependent excitonic fine structure effects, giving rise to thermal equilibria between competitive radiative processes. We believe that the concept of using ligand with strong binding affinity to the surface of the NCs and at the same time having a high solubility in solvents, and organic media in general, can be exploited further for the synthesis of other metal halide NC systems.

■ ASSOCIATED CONTENT

Supporting Information

The Supporting Information is available free of charge at https://pubs.acs.org/doi/10.1021/acs.nanolett.0c03833.

Experimental details, NMR spectra, size distribution histograms, PL emission as a function of the NCs concentration, absorption and PL emission curves, reaction schemes, OLPA-based NCs synthesized at 160 °C, and temperature dependence of the PL fwhm (PDF)

■ AUTHOR INFORMATION

Corresponding Authors

Sergio Brovelli − *Dipartimento di Scienza dei Materiali, Università degli Studi di Milano-Bicocca, 20125 Milano, Italy;* orcid.org/0000-0002-5993-855X; Email: sergio.brovelli@unimib.it

Luca De Trizio − *Nanochemistry Department, Istituto Italiano di Tecnologia (IIT), 16163 Genova, Italy;* orcid.org/0000-0002-1514-6358; Email: luca.detrizio@iit.it

Liberato Manna − *Nanochemistry Department, Istituto Italiano di Tecnologia (IIT), 16163 Genova, Italy;* orcid.org/0000-0003-4386-7985; Email: liberato.manna@iit.it

Authors

Baowei Zhang − *Nanochemistry Department, Istituto Italiano di Tecnologia (IIT), 16163 Genova, Italy; Dipartimento di Chimica e Chimica Industriale, Università degli Studi di Genova, 16146 Genova, Italy*

Luca Goldoni − *Analytical Chemistry Lab, Istituto Italiano di Tecnologia (IIT), 16163 Genova, Italy*

Chiara Lambruschini − *Dipartimento di Chimica e Chimica Industriale, Università degli Studi di Genova, 16146 Genova, Italy*

Lisa Moni − *Dipartimento di Chimica e Chimica Industriale, Università degli Studi di Genova, 16146 Genova, Italy;* orcid.org/0000-0001-5149-2963

Muhammad Imran − *Nanochemistry Department, Istituto Italiano di Tecnologia (IIT), 16163 Genova, Italy;* orcid.org/0000-0001-7091-6514

Andrea Pianetti − *Dipartimento di Scienza dei Materiali, Università degli Studi di Milano-Bicocca, 20125 Milano, Italy*

Valerio Pinchetti − *Dipartimento di Scienza dei Materiali, Università degli Studi di Milano-Bicocca, 20125 Milano, Italy;* orcid.org/0000-0003-3792-3661

Complete contact information is available at: https://pubs.acs.org/10.1021/acs.nanolett.0c03833

Notes

The authors declare no competing financial interest.

■ ACKNOWLEDGMENTS

We thank M. Prato for performing the XPS analyses. We acknowledge funding from the programme for research under

https://dx.doi.org/10.1021/acs.nanolett.0c03833
Nano Lett. 2020, 20, 8847−8853

the Marie Skłodowska-Curie Grant Agreement COMPASS No. 691185 and EPFD0118 CARIPLO 2018 Paternò. We gratefully acknowledge financial support from the Italian Ministry of University and Research (MIUR) through the grants Dipartimenti di Eccellenza-2017 "Materials For Energy" and the Flag-Era JTC2019 project "Solution-Processed Perovskite/Graphene Nanocomposites for Self-Powered Gas Sensors (PeroGaS)".

REFERENCES

(1) Luo, X.; Ding, T.; Liu, X.; Liu, Y.; Wu, K. Quantum-Cutting Luminescent Solar Concentrators Using Ytterbium-Doped Perovskite Nanocrystals. *Nano Lett.* **2019**, *19*, 338−341.

(2) Akkerman, Q. A.; Rainò, G.; Kovalenko, M. V.; Manna, L. Genesis, Challenges and Opportunities for Colloidal Lead Halide Perovskite Nanocrystals. *Nat. Mater.* **2018**, *17*, 394−405.

(3) Shamsi, J.; Urban, A. S.; Imran, M.; De Trizio, L.; Manna, L. Metal Halide Perovskite Nanocrystals: Synthesis, Post-Synthesis Modifications, and Their Optical Properties. *Chem. Rev.* **2019**, *119*, 3296−3348.

(4) Dong, Y.; Wang, Y.-K.; Yuan, F.; Johnston, A.; Liu, Y.; Ma, D.; Choi, M.-J.; Chen, B.; Chekini, M.; Baek, S.-W.; Sagar, L. K.; Fan, J.; Hou, Y.; Wu, M.; Lee, S.; Sun, B.; Hoogland, S.; Quintero-Bermudez, R.; Ebe, H.; Todorovic, P.; Dinic, F.; Li, P.; Kung, H. T.; Saidaminov, M. I.; Kumacheva, E.; Spiecker, E.; Liao, L.-S.; Voznyy, O.; Lu, Z.-H.; Sargent, E. H. Bipolar-Shell Resurfacing for Blue Leds Based on Strongly Confined Perovskite Quantum Dots. *Nat. Nanotechnol.* **2020**, *15*, 668−674.

(5) Liu, Y.; Cui, J.; Du, K.; Tian, H.; He, Z.; Zhou, Q.; Yang, Z.; Deng, Y.; Chen, D.; Zuo, X.; Ren, Y.; Wang, L.; Zhu, H.; Zhao, B.; Di, D.; Wang, J.; Friend, R. H.; Jin, Y. Efficient Blue Light-Emitting Diodes Based on Quantum-Confined Bromide Perovskite Nanostructures. *Nat. Photonics* **2019**, *13*, 760−764.

(6) Li, Z.; Johnston, A.; Wei, M.; Saidaminov, M. I.; Martins de Pina, J.; Zheng, X.; Liu, J.; Liu, Y.; Bakr, O. M.; Sargent, E. H. Solvent-Solute Coordination Engineering for Efficient Perovskite Luminescent Solar Concentrators. *Joule* **2020**, *4*, 631−643.

(7) Chen, Q.; Wu, J.; Ou, X.; Huang, B.; Almutlaq, J.; Zhumekenov, A. A.; Guan, X.; Han, S.; Liang, L.; Yi, Z.; Li, J.; Xie, X.; Wang, Y.; Li, Y.; Fan, D.; Teh, D. B. L.; All, A. H.; Mohammed, O. F.; Bakr, O. M.; Wu, T.; Bettinelli, M.; Yang, H.; Huang, W.; Liu, X. All-Inorganic Perovskite Nanocrystal Scintillators. *Nature* **2018**, *561*, 88−93.

(8) Gandini, M.; Villa, I.; Beretta, M.; Gotti, C.; Imran, M.; Carulli, F.; Fantuzzi, E.; Sassi, M.; Zaffalon, M.; Brofferio, C.; Manna, L.; Beverina, L.; Vedda, A.; Fasoli, M.; Gironi, L.; Brovelli, S. Efficient, Fast and Reabsorption-Free Perovskite Nanocrystal-Based Sensitized Plastic Scintillators. *Nat. Nanotechnol.* **2020**, *15*, 462−468.

(9) Nenon, D. P.; Pressler, K.; Kang, J.; Koscher, B. A.; Olshansky, J. H.; Osowiecki, W. T.; Koc, M. A.; Wang, L.-W.; Alivisatos, A. P. Design Principles for Trap-Free $CsPbX_3$ Nanocrystals: Enumerating and Eliminating Surface Halide Vacancies with Softer Lewis Bases. *J. Am. Chem. Soc.* **2018**, *140*, 17760−17772.

(10) Ten Brinck, S.; Zaccaria, F.; Infante, I. Defects in Lead Halide Perovskite Nanocrystals: Analogies and (Many) Differences with the Bulk. *ACS Energy Lett.* **2019**, *4*, 2739−2747.

(11) Zhang, Y.; Siegler, T. D.; Thomas, C. J.; Abney, M. K.; Shah, T.; De Gorostiza, A.; Greene, R. M.; Korgel, B. A. A "Tips and Tricks" Practical Guide to the Synthesis of Metal Halide Perovskite Nanocrystals. *Chem. Mater.* **2020**, *32*, 5410−5423.

(12) Zhang, B.; Goldoni, L.; Zito, J.; Dang, Z.; Almeida, G.; Zaccaria, F.; de Wit, J.; Infante, I.; De Trizio, L.; Manna, L. Alkyl Phosphonic Acids Deliver $CsPbBr_3$ Nanocrystals with High Photoluminescence Quantum Yield and Truncated Octahedron Shape. *Chem. Mater.* **2019**, *31*, 9140−9147.

(13) Ten Brinck, S.; Infante, I. Surface Termination, Morphology, and Bright Photoluminescence of Cesium Lead Halide Perovskite Nanocrystals. *ACS Energy Lett.* **2016**, *1*, 1266−1272.

(14) Grisorio, R.; Di Clemente, M. E.; Fanizza, E.; Allegretta, I.; Altamura, D.; Striccoli, M.; Terzano, R.; Giannini, C.; Irimia-Vladu, M.; Suranna, G. P. Exploring the Surface Chemistry of Cesium Lead Halide Perovskite Nanocrystals. *Nanoscale* **2019**, *11*, 986−999.

(15) Ravi, V. K.; Santra, P. K.; Joshi, N.; Chugh, J.; Singh, S. K.; Rensmo, H.; Ghosh, P.; Nag, A. Origin of the Substitution Mechanism for the Binding of Organic Ligands on the Surface of $CsPbBr_3$ Perovskite Nanocubes. *J. Phys. Chem. Lett.* **2017**, *8*, 4988−4994.

(16) Imran, M.; Ijaz, P.; Goldoni, L.; Maggioni, D.; Petralanda, U.; Prato, M.; Almeida, G.; Infante, I.; Manna, L. Simultaneous Cationic and Anionic Ligand Exchange for Colloidally Stable $CsPbBr_3$ Nanocrystals. *ACS Energy Lett.* **2019**, *4*, 819−824.

(17) Krieg, F.; Ochsenbein, S. T.; Yakunin, S.; Ten Brinck, S.; Aellen, P.; Süess, A.; Clerc, B.; Guggisberg, D.; Nazarenko, O.; Shynkarenko, Y.; Kumar, S.; Shih, C.-J.; Infante, I.; Kovalenko, M. V. Colloidal $CsPbX_3$ (X = Cl, Br, I) Nanocrystals 2.0: Zwitterionic Capping Ligands for Improved Durability and Stability. *ACS Energy Lett.* **2018**, *3*, 641−646.

(18) Protesescu, L.; Yakunin, S.; Bodnarchuk, M. I.; Krieg, F.; Caputo, R.; Hendon, C. H.; Yang, R. X.; Walsh, A.; Kovalenko, M. V. Nanocrystals of Cesium Lead Halide Perovskites ($CsPbX_3$, X = Cl, Br, and I): Novel Optoelectronic Materials Showing Bright Emission with Wide Color Gamut. *Nano Lett.* **2015**, *15*, 3692−3696.

(19) Butkus, J.; Vashishtha, P.; Chen, K.; Gallaher, J. K.; Prasad, S. K. K.; Metin, D. Z.; Laufersky, G.; Gaston, N.; Halpert, J. E.; Hodgkiss, J. M. The Evolution of Quantum Confinement in $CsPbBr_3$ Perovskite Nanocrystals. *Chem. Mater.* **2017**, *29*, 3644−3652.

(20) Rossi, D.; Liu, X.; Lee, Y.; Khurana, M.; Puthenpurayil, J.; Kim, K.; Akimov, A. V.; Cheon, J.; Son, D. H. Intense Dark Exciton Emission from Strongly Quantum-Confined $CsPbBr_3$ Nanocrystals. *Nano Lett.* **2020**, *20*, 7321−7326.

(21) Becker, M. A.; Vaxenburg, R.; Nedelcu, G.; Sercel, P. C.; Shabaev, A.; Mehl, M. J.; Michopoulos, J. G.; Lambrakos, S. G.; Bernstein, N.; Lyons, J. L.; Stöferle, T.; Mahrt, R. F.; Kovalenko, M. V.; Norris, D. J.; Rainò, G.; Efros, A. L. Bright Triplet Excitons in Caesium Lead Halide Perovskites. *Nature* **2018**, *553*, 189−193.

(22) Rawn, J. D.; Ouellette, R. J. *Organic Chemistry: Structure, Mechanism, Synthesis*; Elsevier: San Diego, CA, 2014.

(23) De Roo, J.; Zhou, Z.; Wang, J.; Deblock, L.; Crosby, A. J.; Owen, J. S.; Nonnenmann, S. S. Synthesis of Phosphonic Acid Ligands for Nanocrystal Surface Functionalization and Solution Processed Memristors. *Chem. Mater.* **2018**, *30*, 8034−8039.

(24) Smock, S. R.; Williams, T. J.; Brutchey, R. L. Quantifying the Thermodynamics of Ligand Binding to $CsPbBr_3$ Quantum Dots. *Angew. Chem.* **2018**, *130*, 11885−11889.

(25) Gomes, R.; Hassinen, A.; Szczygiel, A.; Zhao, Q.; Vantomme, A.; Martins, J. C.; Hens, Z. Binding of Phosphonic Acids to Cdse Quantum Dots: A Solution Nmr Study. *J. Phys. Chem. Lett.* **2011**, *2*, 145−152.

(26) Owen, J. S.; Park, J.; Trudeau, P.-E.; Alivisatos, A. P. Reaction Chemistry and Ligand Exchange at Cadmium-Selenide Nanocrystal Surfaces. *J. Am. Chem. Soc.* **2008**, *130*, 12279−12281.

(27) Woo, J. Y.; Lee, S.; Lee, S.; Kim, W. D.; Lee, K.; Kim, K.; An, H. J.; Lee, D. C.; Jeong, S. Air-Stable PbSe Nanocrystals Passivated by Phosphonic Acids. *J. Am. Chem. Soc.* **2016**, *138*, 876−883.

(28) Saran, R.; Heuer-Jungemann, A.; Kanaras, A. G.; Curry, R. J. Giant Bandgap Renormalization and Exciton-Phonon Scattering in Perovskite Nanocrystals. *Adv. Opt. Mater.* **2017**, *5*, 1700231.

(29) Shi, H.; Zhang, X.; Sun, X.; Chen, R.; Zhang, X. Direct and Indirect Recombination and Thermal Kinetics of Excitons in Colloidal All-Inorganic Lead Halide Perovskite Nanocrystals. *J. Phys. Chem. C* **2019**, *123*, 19844−19850.

(30) Sebastian, M.; Peters, J. A.; Stoumpos, C. C.; Im, J.; Kostina, S. S.; Liu, Z.; Kanatzidis, M. G.; Freeman, A. J.; Wessels, B. W. Excitonic Emissions and Above-Band-Gap Luminescence in the Single-Crystal Perovskite Semiconductors $CsPbBr_3$ and $CsPbCl_3$. *Phys. Rev. B: Condens. Matter Mater. Phys.* **2015**, *92*, 235210.

https://dx.doi.org/10.1021/acs.nanolett.0c03833
Nano Lett. 2020, 20, 8847−8853

(31) Cheng, O. H.-C.; Qiao, T.; Sheldon, M.; Son, D. H. Size- and Temperature-Dependent Photoluminescence Spectra of Strongly Confined $CsPbBr_3$ Quantum Dots. *Nanoscale* **2020**, *12*, 13113−13118.
(32) Ramade, J.; Andriambariarijaona, L. M.; Steinmetz, V.; Goubet, N.; Legrand, L.; Barisien, T.; Bernardot, F.; Testelin, C.; Lhuillier, E.; Bramati, A.; Chamarro, M. Exciton-Phonon Coupling in a $CsPbBr_3$ Single Nanocrystal. *Appl. Phys. Lett.* **2018**, *112*, 072104.
(33) Lao, X.; Yang, Z.; Su, Z.; Wang, Z.; Ye, H.; Wang, M.; Yao, X.; Xu, S. Luminescence and Thermal Behaviors of Free and Trapped Excitons in Cesium Lead Halide Perovskite Nanosheets. *Nanoscale* **2018**, *10*, 9949−9956.
(34) Wu, W.; Liu, W.; Wang, Q.; Han, Q.; Yang, Q. Temperature-Dependent Photoluminescence of Pure and Mn-Doped $CsPbCl_3$ Nanocrystals. *J. Alloys Compd.* **2019**, *787*, 165−172.

https://dx.doi.org/10.1021/acs.nanolett.0c03833
Nano Lett. 2020, 20, 8847−8853